ChemPubSoc Europe

DOI: 10.1002/cssc.201403024

CHEMSUSCHEM Full Papers

VIP

How a $[Co^{IV}{=}O]^{2+}$ Fragment Oxidizes Water: Involvement of a Biradicaloid $[Co^{II}–(\cdot O\cdot)]^{2+}$ Species in Forming the O–O Bond

Douglas W. Crandell,[a] Soumya Ghosh,[a] Curtis P. Berlinguette,*[b] and Mu-Hyun Baik*[a, c]

The mechanism of water oxidation performed by a recently discovered cobalt complex $[Co(Py5)(OH_2)](ClO_4)_2$ (**1**; Py5 = 2,6-(bis(bis-2-pyridyl)-methoxymethane)pyridine) was examined using quantum chemical models based on density functional theory. The computer models were first benchmarked against the experimental cyclic voltammetry data to identify the catalytically competent resting state of the catalyst, which was thought to contain a Co^{IV}–oxyl complex. The electronic structure calculations suggest that the low-spin doublet state is energetically most favorable, but the catalytically most active species is the intermediate-spin quartet complex that is almost isoenergetic with the doublet state. The electronic structure of the quartet state shows significant spin polarization on the terminal oxygen atom, which is consistent with an intramolecular electron transfer from the oxygen to the metal. Based on the calculated spin densities, the formally $[Co^{IV}{=}O]$ can be viewed as a biradicaloid $[Co^{II}–(\cdot O\cdot)]^{2+}$, that is, a cobalt–oxene moiety. This electronic structure is reminiscent of many other systems where similar electronic patterns were proposed to be responsible for the oxidative reactivity. In this context, this first-row transition-metal system constitutes a logical extension, because the oxyl-radical character is maximized by using the more easily accessible high-spin configurations in which two half-filled Co–dπ orbitals can work in concert to maximize the oxyl-radical character to ultimately afford a new reactive intermediate that can be characterized as carrying a biradicaloid oxene moiety with a formal oxidation state of zero. This conceptual proposal for the catalytically active species provides a plausible rationale for the remarkable oxidative reactivity.

Introduction

Solar energy is the most attractive renewable energy source to combat our current dependence on fossil fuels and reduce the rising levels of greenhouse gases in the atmosphere.[1,2] Artificial photosynthesis represents a key technology that can transform carbon dioxide into solar fuels.[3,4] Water is the most viable candidate for a practically unlimited source of electrons that are needed for the reduction of CO_2. Nature employs a Mn_4CaO_5 cluster[5] in the oxygen-evolving complex of photosystem II to oxidize water and much research has been dedicated to synthetic multinuclear water oxidation catalysts,[6–17] which mimic its reactivity. Homogeneous, mononuclear water oxidation catalysts are a more recent development;[12,18–22] especially those based on first-row, earth-abundant metals, including iron,[23–25] and cobalt.[26,27] Only a few mechanistic computational studies have been performed on homogeneous first-row catalysts[28–30] and mechanistic insights generally remain lacking.

One of us recently reported a novel water oxidation catalyst, $[Co(Py5)(OH_2)](ClO_4)_2$ (**1**; Py5 = 2,6-(bis(bis-2-pyridyl)-methoxymethane)pyridine), containing only a single Co center[31] and displaying remarkable stability against decomposition over the pH range of 7.6–10.3.[32] Electrocatalytic turnover can be observed at pH 9.2 indicated by a sharp rise in voltammetric current at approximately 1.4 V versus NHE, which correlates to an overpotential of only about 0.5 V, one of the lowest reported for a synthetic water oxidation catalyst. Two oxidation processes were observed in the cyclic voltammogram of **1**: (i) a single, pH-dependent, reversible oxidation at 0.75 V at pH 2.2, (ii) a second oxidation at 1.43 V within a pH range of 7.6–10.3, which becomes pH-dependent at pH > 10.3. The first oxidation process was assigned to the $[Co^{III}–OH]^{2+}/[Co^{II}–OH_2]^{2+}$ redox couple, whereas the second oxidation was thought to be associated with the formation of a $[Co^{IV}–OH]^{3+}$ species.

To promote productive design strategies for improved catalysts it is necessary to understand how only one metal center can accomplish this difficult reaction; in particular, it is important to understand which electronic feature allows the metal center to overcome the challenge of forming the O–O bond. Typically, a high-valent metal oxo species is proposed to

[a] D. W. Crandell, S. Ghosh, M.-H. Baik
Department of Chemistry
Indiana University
800 E. Kirkwood Avenue, Bloomington, IN 47405, (USA)
E-mail: mbaik@indiana.edu

[b] C. P. Berlinguette
Department of Chemistry
University of British Columbia
2036 Main Mall, Vancouver, BC V6T 1Z1 (Canada)
E-mail: cberling@chem.ubc.ca

[c] M.-H. Baik
Department of Materials Chemistry
Korea University
Jochiwon-eup, Sejong-si, 339-700 (South Korea)

Supporting Information for this article is available on the WWW under http://dx.doi.org/10.1002/cssc.201403024.

couple with water to form the O–O bond[33] and it is a demanding task, as each of the oxygen atoms are formally in a −II oxidation state. It has been proposed, however, that oxyl radical intermediates are necessary for O–O bond formation in the multinuclear Mn-based complex of Photosystem II.[34,35] In previous work, we found that the terminal oxo moiety in a formally Ru^{V}=O fragment can also adopt this non-classical electronic structure,[36] where an intramolecular electron transfer from the oxo to the metal center takes place to afford what is better described as a Ru^{IV}–O· moiety. The O–O bond formation is promoted by the radicaloid oxyl-group attacking another oxygen fragment in a radical-recombination type of a reaction.[37–39] Subsequent work confirmed that these mechanistic interpretations are plausible and in good agreement with experimental findings.[40–43] It is both challenging and interesting to consider the redox catalytic mechanisms of first-row metal systems, which possess more complex electronic structures by virtue of having accessible high spin states. Mononuclear catalysts also present an additional challenge as only one metal center can store the necessary oxidizing equivalents. This work investigates the unique electronic structure possessed by a single cobalt center with aims of understanding the features that facilitate water oxidation.

Computational Details

All calculations were carried out using density functional theory[44,45] (DFT) as implemented in the Jaguar 7.7 suite of ab initio quantum chemistry programs.[46] Geometries were optimized with the B3LYP[47–51] functional using the 6-31G** basis set with Co represented by the Los Alamos LACVP basis set.[52,53] Single point energies were computed from the optimized geometries using Dunning's correlation-consistent triple-ζ basis set, cc-pVTZ(-f),[54] where Co was represented using a modified version of LACVP, designated as LACV3P with decontracted exponents. Vibrational frequencies computed at the B3LYP/6-31G** level of theory were used to derive zero point energy and vibrational entropy corrections from unscaled frequencies. Entropy here refers specifically to the vibrational/rotational/translational entropy of the solute(s), as the continuum model includes the entropy of the solvent. All intermediates were confirmed to be minima possessing zero imaginary frequencies and all transition states were confirmed as saddle points having only one imaginary frequency. Solvation energies were calculated at the double-ζ level using a dielectric constant $\varepsilon = 80.37$ for water. Solvation calculations were done using a self-consistent reaction field approach (SCRF),[55–57] on numerical solutions of the Poisson–Boltzmann equation.[58] As with all continuum models, the solvation energies are subject to empirical parameterization of the atomic radii that are used to generate the solute surface. The energy components have been computed with the following protocol. The free energy in solution phase G(sol) has been calculated as follows:

$$G(\text{sol}) = G(\text{gas}) + G(\text{solv}) \quad (1)$$

$$G(\text{gas}) = H(\text{gas}) - TS(\text{gas}) \quad (2)$$

$$H(\text{gas}) = E(\text{SCF}) + \text{ZPE} \quad (3)$$

$$\Delta E(\text{SCF}) = \sum E(\text{SCF}) \text{ for products} - \sum G(\text{SCF}) \text{ for reactants} \quad (4)$$

$$\Delta G(\text{sol}) = \sum G(\text{sol}) \text{ for products} - \sum G(\text{sol}) \text{ for reactants} \quad (5)$$

G(gas) is the free energy in gas phase; H(gas) is the enthalpy in gas phase; T is the temperature (298 K); S(gas) is the entropy in gas phase; E(SCF) is the self-consistent field energy, that is, "raw" electronic energy as computed from the SCF procedure and ZPE is the zero point energy. For computations involving proton-coupled redox reactions, it is necessary to account for the free energy of a proton in solution. We used the following expression to compute $G(H^+)$, the free energy of a proton in solution:

$$G(H^+) = H^{gas}(H^+) - TS + {}^5/_2 RT + G^{solv}(H^+) \quad (6)$$

where $H^{gas}(H^+)$, the gas-phase electronic energy, is zero by definition; R is the gas constant; T is 298.15 K; S is the translational entropy of a free hydrogen atom calculated using the Sackur–Tetrode equation (26.04 eu); ${}^5/_2 RT$ is the thermal correction, which amounts to 0.064 eV at 298.15 K; and $G^{solv}(H^+)$ is the free energy of solvation of a proton (−265.9 kcal mol^{-1}).[59,60] Since experimental redox potentials are reported at pH 2.2 and 9.2, our computed standard redox potentials were adjusted to the experimental pH conditions using the Nernst equation:

$$E_{1/2}(\text{calcd})_{\text{pH}} = E^{\circ}_{1/2}(\text{calcd}) - \frac{RT\ln(10)}{n_e} \times n_{H^+} \times \text{pH} \quad (7)$$

Where n_e and n_{H^+} are the numbers of electrons and protons, respectively. The value of RT is computed to be 0.0257 V at 298.15 K; thus, according to Equation (5), ≈0.13 V and ≈0.54 V should be subtracted from the computed standard redox potentials when one proton is involved in the redox reaction at pH 2.2 and 9.2, respectively. To account for the energy required to generate a hydroxide ion at pH 9.2 an additional 0.54 V (12.51 kcal mol^{-1}) is added to the kinetic barriers for hydroxide attack on the proposed reactive intermediate **3**.

Please note: Coordinates of all calculated structures, and energy components are available in the online Supporting Information.

Results and Discussion

Before different possible mechanistic scenarios can be compared to each other, it is important to identify intermediates that may serve as the starting point of the electrocatalytic cycle. In the current case, identifying the catalytically competent species is particularly interesting, because it is proposed to be a Co^{IV} species.[31] Whereas Co^{IV} has been implicated to play an important role in other water oxidation reactions,[61–64] not much is known about Co^{IV} species within a homogeneous

catalyst context as direct spectroscopic evidence is rare.[65] Ideally, both computational and experimental results should converge to an unambiguous conclusion, such that the catalytically competent intermediate can be used as a benchmark for connecting the quantum calculations to experiments. Unfortunately, the key intermediates of catalytic cycles are by default highly reactive, short lived, and often evade precise detection, making it necessary to utilize indirect observables to benchmark our computational results against experiments. In previous work, we demonstrated that density functional calculations can be used successfully to compute redox potentials of transition metal complexes.[66] While these calculations remain challenging, the computational protocol is sufficiently robust that good correlation between experimental and calculated potentials indicates that the most salient features of the redox-active intermediate may have been captured in the quantum chemical model. Conversely, disagreements that are greater than 150 mV suggest that the composition of the redox pairs assumed in the theoretical model may be different from what gave rise to the experimental potentials. In short, redox potentials are useful benchmarks to challenge and refine the computer model against experiments.

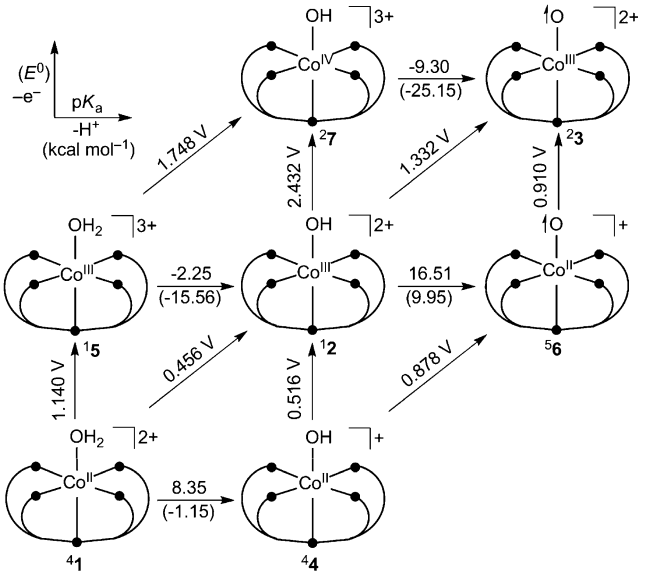

Scheme 1. Relative energies of the most relevant intermediates for the transfer of two electrons and two protons at pH 9.2.

Table 1. Experimental and computed potentials of ^{4}**1** in *V* vs. NHE.

	$[Co^{III}–OH]^{2+}$(^{1}**2**)/$[Co^{II}–OH_2]^{2+}$(^{4}**1**) (pH 2.2)	$[Co^{IV}–O]^{2+}$(^{2}**3**)/$[Co^{III}–OH]^{2+}$(^{1}**2**) (pH 9.2)
experimental	$E_1^\circ = 0.75$	$E_2^\circ \approx 1.43$
computed	$E_1^\circ = 0.869$	$E_2^\circ = 1.332$

Table 1 compares the two redox potentials of **1** observed experimentally using cyclic voltammetry (CV) to DFT-calculated potentials. The first oxidation, seen as an electrochemically reversible event at $E_1^\circ = 0.75$ V at pH 2.2,[31] was previously assigned to a proton-coupled oxidation involving the redox pair $[Co^{III}–OH]^{2+}/[Co^{II}–OH_2]^{2+}$.[67] Our calculations confirm this assignment and predict a redox potential of 0.869 V, in reasonable agreement with the CV data. The second oxidation is electrochemically irreversible, catalytically enhanced and is seen at an anodic peak potential E_2^p at ~1.43 V. As there is no cathodic wave in the CV, it is not possible to obtain the normal redox potential E_2° for this process using standard electrochemical techniques. Assuming standard electrochemical and chemical reaction kinetics, it is plausible to assume therefore that 1.43 V is the upper limit estimate for the associated normal redox potential. This information is helpful for evaluating our computed potential for this process: Our calculations only yield the normal redox potential E_2° because we evaluate the thermodynamics of the redox pairs, disregarding kinetic phenomena and other processes that render the redox reaction irreversible. The DFT-calculated redox potential for the proton-coupled electron transfer (PCET) involving the redox couple $[Co^{III}–OH]^{2+}$ to $[Co^{IV}–O]^{2+}$ is 1.332 V at pH 9.2, in good agreement with the experimental observations discussed above. Although no pH dependence of the potential was observed within a relatively narrow pH window experimentally, we suggest that the second redox event is proton coupled. The simple one-electron oxidation of $[Co^{III}–OH]^{2+}$ to $[Co^{IV}–OH]^{3+}$ is calculated to occur at a normal potential of 2.432 V, which is much too high. Our calculations estimate the pK_a of the putative $[Co^{IV}–OH]^{3+}$ species to be −9.3. Thus, a plausible justification for not observing a pH dependent behavior in experiments is that the deprotonation is rapid, such that it cannot be observed within the time scale of the electrochemical measurement.

Based on the pH dependence of the first redox couple, the process was previously assigned as a PCET between $[Co^{II}–OH_2]^{2+}$ and $[Co^{III}–OH]^{2+}$. Scheme 1 visualizes the relative energies of the most relevant intermediates for the transfer of two electrons and two protons at pH 9.2. The quartet state for the starting complex $[Co^{II}–OH_2]^{2+}$ **1** is favored over the doublet state by 5.3 kcal mol^{-1}. Beginning from the dicationic quartet ground state ^{4}**1**, the removal of electrons is illustrated in the vertical direction and the deprotonation events are arranged along the horizontal line to allow for the proton-coupled electron transfer energy to be shown on the diagonal lines. The calculated pK_a values of each species are listed on top of the horizontal arrows, whereas the pH-adjusted free energy associated with the deprotonation is given underneath the horizontal arrows. At the experimental pH of 9.2, the initial complex ^{4}**1**, with a computed pK_a of 8.35, is expected to establish an equilibrium that slightly favors the deprotonated $[Co^{II}–OH]^+$ containing ^{4}**4** state. Removal of a single electron from ^{4}**1** is expected to lead to a spin crossover into the low-spin manifold at the Co^{III}-d^6 center,[68] possibly giving rise to the intermediates ^{1}**5** and ^{1}**2**. The high-spin analogues of these Co^{III} species

lie 31.1 and 6.7 kcal mol^{-1} higher in energy, respectively. Our calculations suggest that the aqua ligand at the axial coordination site in ^{1}**5** is highly acidic with a predicted pK_a of −2.25. Thus, at pH 9.2 the Gibbs free energy of deprotonation becomes −15.56 kcal mol^{-1}. Taken together, we expect intermediate ^{1}**2** to be the dominant 1-electron reduced intermediate.

To generate the reactive intermediate bearing the proposed catalytically competent $[Co^{IV}{=}O]^{2+}$ fragment, an additional electron must be removed from ^{1}**2**, which takes place as another PCET event. As discussed above, the $[Co^{IV}{-}OH]^{3+}$ species is expected to rapidly deprotonate to give the $[Co^{IV}{=}O]^{2+}$ species ^{2}**3**. This second oxidation step is predicted to occur at a normal oxidation potential of 1.332 V and the doublet and quartet spin states of the formally Co(IV)-d^5 intermediate, ^{2}**3** and ^{4}**3**, are calculated to be practically isoenergetic with the energy difference being only 1.1 kcal mol^{-1} in favor of the doublet state. The electronic structure of ^{2}**3** is best represented as $Co^{III}{-}O\cdot$ rather than $Co^{IV}{=}O$ according to the Mulliken spin densities, which show no unpaired electrons on Co and one unpaired electron (0.997) on O. This electronic structure is very reminiscent of what was found for Meyer's blue dimer, where we proposed that the catalytically active species contained a $Ru^{IV}{-}O\cdot$ fragment.[37]

Assuming that ^{2}**3**/^{4}**3** are the catalytically competent intermediates, the key mechanistic question becomes whether the key O–O bond forming reaction is an intra or inter-molecular event. In other words, does the hydroxide substrate first bind to the Co center to form an adduct or does species **3** interact with a free hydroxide anion? For the hydroxide-adduct to form, one of the Co–pyridyl bonds must be cleaved, leaving a coordination site vacant. Given the well documented inertness of high valent Co towards ligand exchange,[69] it is unreasonable for such a process to happen for intermediate **3**. Instead, the most likely stage at which one of the pyridyl ligands will be replaced with an oxo-carrying ligand, which may be an aqua or a hydroxo ligand, is prior to the electrochemical step. Intermediate ^{4}**1** is formally a 19-electron species with a high-spin configuration at the Co^{II} center with two electrons placed in metal-N σ*-orbitals. Thus, the ligand-exchange reaction should be easy to accomplish.[70] The axial pyridine ligand *trans* to the aqua ligand is protected by the chelate effect, but the equatorial pyridines can rotate relatively easily around C–C σ bonds connecting them to the methylene carbons of the Py5 backbone, which should render them vulnerable to ligand-exchange. Recently, the instability of the Co^{II}–pyridyl bond was documented in a similar complex based on NMR data.[71]

The energy profile for the detachment of an equatorial pyridine and coordination of a hydroxide ion is shown in Figure 1. The barrier for cleavage of an equatorial Co–N bond on the $S=3/2$ potential energy surface is only 18.73 kcal mol^{-1} (^{4}**1-TS**) and can be readily overcome under ambient conditions to give a five-coordinate square pyramidal intermediate that is approximately 9.1 kcal mol^{-1} above ^{4}**1**. The high- and low-spin intermediates ^{4}**8** and ^{2}**8** are nearly isoenergetic, but the hydroxo-adduct intermediates, where the vacant coordination site is occupied by an OH^- ligand are significantly different in energy. The high-spin complex ^{4}**9** is 11.96 kcal mol^{-1} lower than

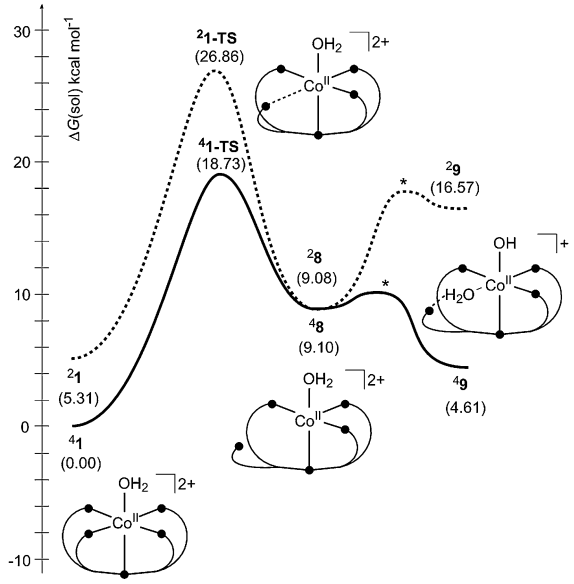

Figure 1. Energetic requirements for replacing pyridine ligand with hydroxide.

the low-spin analogue ^{2}**9**, which is easy to understand, as the anionic hydroxo ligand should decrease the ligand field splitting D_q at the Co^{II} center. Interestingly, the hydroxide ion prefers the axial position and the aqua moiety is pushed to the equatorial binding site, hydrogen bonding with the uncoordinated pyridine fragment (Figure 1). This alternative intermediate ^{4}**9** is only 4.6 kcal mol^{-1} higher in energy than ^{4}**1**, indicating that there exists a viable intermediate with two oxygen based ligands coordinated in a *cis* fashion potentially allowing for intramolecular O–O bond forming to be competitive with intermolecular O–O bond formation.

Calculated electrochemical properties of ^{4}**9** are summarized in Scheme 2. The proton-coupled oxidation ^{4}**9** to form the 1-

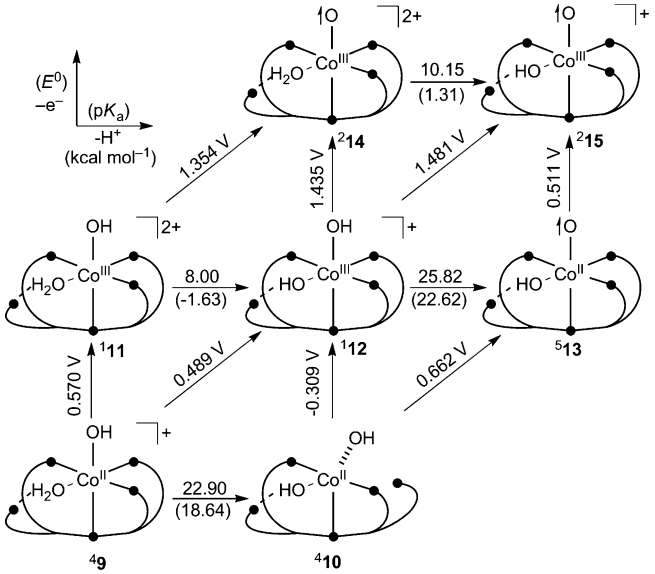

Scheme 2. Calculated electrochemical properties of ^{4}**9**.

electron oxidized intermediate ^{1}**12** is predicted to be 0.489 V, which is nearly identical to the 0.456 V for the analogous oxidation of ^{4}**1**. The potential for oxidizing ^{1}**12** is found to be 1.481 V, which is notably higher than the oxidation potential of 1.332 V calculated for ^{1}**2**, but this value is still sufficiently close to the experimentally determined peak potential of ~1.43 V and we cannot rule out a mechanistically relevant role of the intermediate ^{4}**9**; complex ^{2}**15** may therefore be a suitable candidate for promoting the intramolecular formation of the O–O bond. Thermodynamically, ^{2}**15** is only 8.83 kcal mol^{-1} higher in energy than ^{2}**3**, the analogous fully oxidized Co^{IV} complex with all five Co-pyridyl bonds intact.

Mechanism of O–O bond formation

Experimental kinetics studies were consistent with a mechanism that was first order with respect to both catalyst and hydroxide concentrations,[32] thus discounting a radical coupling mechanism between two cobalt oxo species. Therefore, we focused our efforts on two principal scenarios: intermolecular nucleophilic attack of water or hydroxide on the $[Co^{IV}{=}O]^{2+}$ species ^{2}**3** or an intramolecular coupling between the oxo and hydroxyl ligands in ^{2}**15**. Although ^{2}**15** starts initially at a higher energy for forming the O–O bond, there is no translational entropy penalty for the intramolecular O–O coupling, which may provide a sufficient amount of energy to render the intramolecular mechanism competitive. Figure 2 compares the inter- and intramolecular routes on both the doublet and quartet surfaces. The intermolecular pathways are shown as solid lines, whereas the intramolecular mechanisms are represented by broken lines. The doublet surface is shown in gray and the quartet surface is given in black. The lowest energy pathway is an intermolecular nucleophilic attack of hydroxide on the quartet spin surface with a solution phase activation free energy of 21.1 kcal mol^{-1}. The calculated transition state ^{4}**3-TS** is shown in Figure 3. The O–O distance in the transition state is 2.439 Å and the hydroxide attacks the Co-oxygen atom in a "side-on" fashion, maintaining some hydrogen-bonding character. The analogous transition state on the doublet surface was found to be mechanistically irrelevant with a barrier of 33.2 kcal mol^{-1}. Not surprisingly, the Co^{II}-d^{7} center in the final hydroperoxo product prefers the high-spin configuration and ^{4}**16** is 10.7 kcal mol^{-1} lower in energy than its low-spin analogue ^{2}**16**.

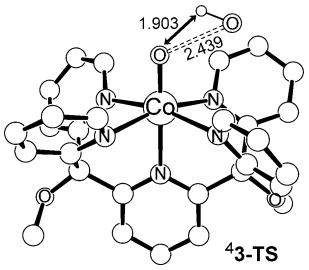

Figure 3. Structure of ^{4}**3-TS**.

The barrier for the intramolecular coupling of the hydroxyl and oxo ligands in ^{4}**15** is calculated to be 29.9 kcal mol^{-1}. Coincidentally, this barrier is equivalent to the sum of the intermolecular O–O coupling barrier of 21.1 kcal mol^{-1} and the preparation energy of species ^{2}**15** of 8.8 kcal mol^{-1}, suggesting that an intramolecular O–O bond formation event could take place if a ligand could be designed permitting two oxygen-containing ligands to occupy two *cis* positions while stabilizing the highly reactive Co^{IV} metal center. In other words, the inter and intramolecular O–O coupling transition states are energetically equivalent in principle and the intermolecular mechanism is preferred in this case because of the non-productive energy penalty caused by the coordination of the hydroxide reactant. Interestingly, both the doublet and quartet states give nearly identical barriers of the intramolecular O–O coupling, which is in stark contrast to the intermolecular coupling, where the quartet state displays a decisive advantage. In addition to these plausible O–O coupling mechanisms, we also considered an intermolecular nucleophilic attack of a hydroxide ion on $[Co^{IV}(O)(OH)_2]^{2+}$, ^{2}**14**, which is the conjugate acid of ^{2}**15** and explored if nucleophilic attack of a water molecule on ^{4}**3** provides reasonable barriers. We found that the barriers are much too high with the former being at 32.6 and the latter at 41.0 kcal mol^{-1}. Thus, these reaction pathways can be excluded from further consideration.

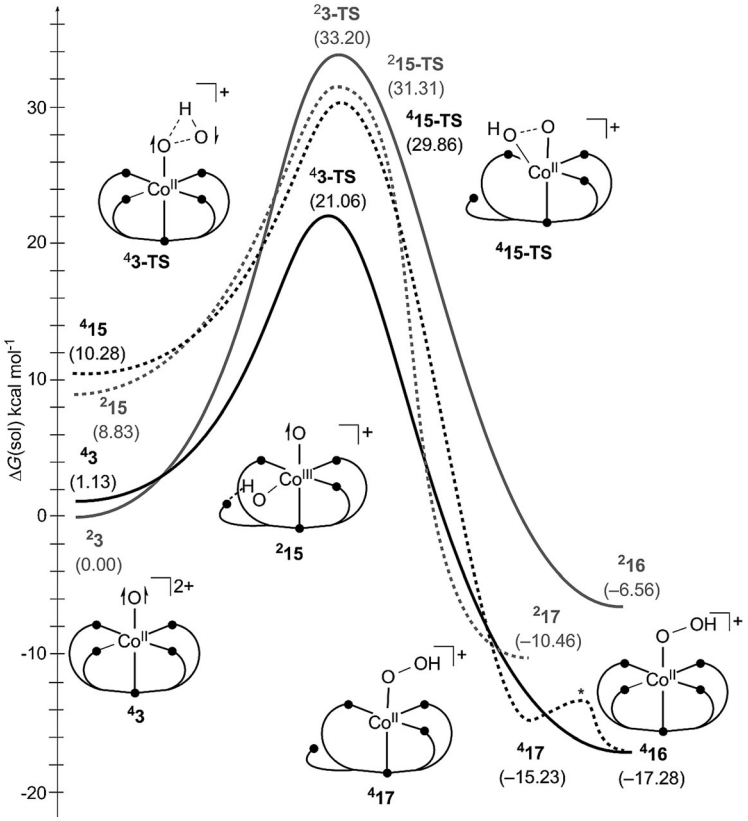

Figure 2. Energy profile for the formation of the O–O bond.

Electronic structure

The DFT-optimized structures and schematic representations of the molecular orbital (MO) diagrams for the initial $[Co^{II}–OH_2]^{2+}$ complex **1** as well as the putative $[Co^{IV}{=}O]^{2+}$ intermediate **3** are shown in Figure 4. The high-spin and low-spin configurations of the Co^{II}-d^7 centered within the approximately octahedral coordination geometry were considered to afford the quartet and doublet intermediates ^{4}**1** and ^{2}**1**, respectively. Complex ^{4}**1** shows an elongation of the Co–N2 and Co–N4 bonds to 2.256 Å that is consistent with a 1st order Jahn–Teller-like distortion arising from asymmetric occupation of the t_{2g}-like d_{xz} and d_{yz} orbitals. Complex ^{4}**3** also exhibits a similar effect via elongations of the Co–N2 and Co–N4 bond distances shown in Table 2 to 2.309 Å coincident with a contraction of the Co–O bond length from 1.760 Å to 1.637 Å in order to relieve the degeneracy of the unevenly occupied e_g-like orbitals.

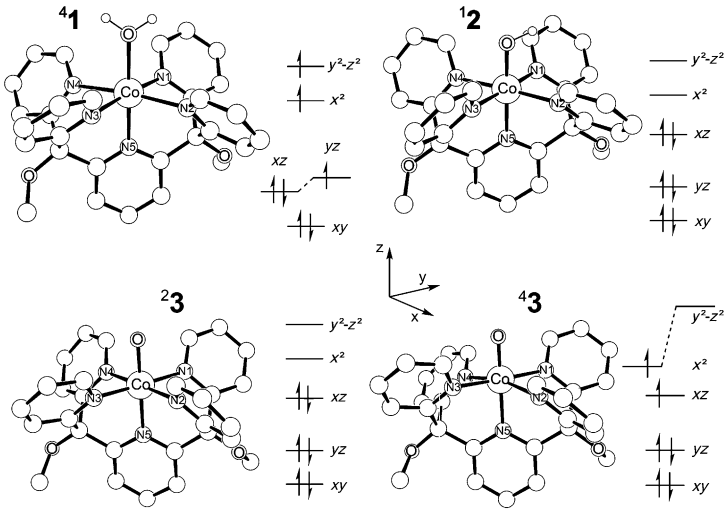

Figure 4. DFT-optimized structures of ^{4}**1**, ^{1}**2**, ^{2}**3** and ^{4}**3** with corresponding molecular orbital occupations.

Table 2. Calculated M–L bond lengths for ^{4}**1**, ^{1}**2**, ^{2}**3**, and ^{4}**3** in Å.

Bond	^{4}**1**	^{1}**2**	^{2}**3**	^{4}**3**
Co–N1	2.257	2.035	2.056	2.025
Co–N2	2.154	2.006	2.028	2.309
Co–N3	2.256	2.013	2.031	2.026
Co–N4	2.151	1.996	2.032	2.309
Co–N5	2.073	2.007	1.973	1.998
Co–O	2.150	1.842	1.760	1.637

The most difficult step in water oxidation is commonly associated with O–O coupling and it is therefore important to understand how this step is accomplished. Here, the O–O coupling transition state is found at only 21 kcal mol^{-1}, which is remarkably low. In the "blue dimer"[6] we found previously that the formally $[Ru^V{=}O]$ fragments adopt an electronic structure that is more consistent with $[Ru^{IV}–O\cdot]$ moieties,[37] allowing the oxyl radical to attack a water molecule with ease. In another case, redox non-innocent quinone ligands assisted this process by allowing two Ru-centers to develop $[Ru^{III}–O\cdot]$ character and engage in intramolecular O–O coupling.[38,72,73] Many other systems[28,35,43,74–78] have been identified with similar electronic structure patterns and there is now a growing consensus on the role of metal-bound oxyl radicals in water oxidation. From a fundamental mechanistic perspective, the catalytic cycle proposed above is unusual, because the O–O bond is formed between a metal-bound oxo and a free hydroxide anion: As the metal-bound oxos are typically in a (−II) or (−I) oxidation state, the most natural reaction partner for an intermolecular O–O coupling is a neutral water molecule, minimizing the Coulombic repulsions between the two oxygen atoms. The fact that the O–O coupling can be accomplished with a barrier of only 21 kcal mol^{-1}, despite the anticipated electrostatically unfavorable interaction, points to an unusual electronic structure that must be particularly potent in oxidizing the hydroxyl reactant.

In good agreement with our previous work, the ^{2}**3** intermediate is best described as $[Co^{III}–(O\cdot)]^{2+}$, with a Mulliken spin density of 0.997 on the O atom, indicating a significant oxyl radical character on oxygen. More interestingly, the intermediate ^{4}**3** that is the most active species for O–O bond formation, is a diradicaloid metal–oxene species $[Co^{II}–(\cdot O\cdot)]^{2+}$ with a spin density of 1.113 on oxygen. A single unpaired electron can be typically correlated with a Mulliken population of approximately 0.6; thus, the terminal oxygen atom can be viewed as adopting a formal oxidation state of zero, which provides an intuitive justification for why intermediate ^{4}**3** reacts readily with the hydroxide substrate. Iron-bound oxene has long been recognized as highly oxidizing, for example in cytochrome P450;[79–82] but this is the first instance where a cobalt-bound oxene is invoked in a small complex. The most important frontier orbitals of ^{4}**3** are shown in Figure 5, in which natural bond orbitals are used.[83,84] Among the α-MOs, the five Co-centered d-orbitals are easily identified; as expected, the d_{xy}, d_{yz}, d_{xz} and d_{x^2} orbitals are occupied and $d_{y^2-z^2}$ is empty. The two lone-pair orbitals of oxygen, O-p_x and O-p_y, are also found to be pure valence lone-pair orbitals, as illustrated in Figure 5a. In the β-MO space, only one purely metal-based d-orbital that is identical to the α-d_{xy} orbital is occupied, thus indicating that the d_{xy} orbital is doubly occupied. As shown in Figure 5b, there are two occupied β-MOs that are derived from the d_{xz} and d_{yz} orbitals with strong Co–O π-bonding interactions, whereas the corresponding π*-orbitals dominated by O-p_x and O-p_y orbitals are empty. The β-MOs in Figure 5b constitute the electronic foundation for the aforementioned Co–oxene character: The highly oxidizing nature of a Co^{IV}-d^5 center in the quartet configuration is expressed in the ability of the two β-MOs based on the Co-d_{xz} and d_{yz} orbitals, which would be empty in the quartet Co^{IV}-d^5 configuration, to pull the O-p_x and O-p_y electrons into the metal center using the Co–O π-bonding interactions. This β-

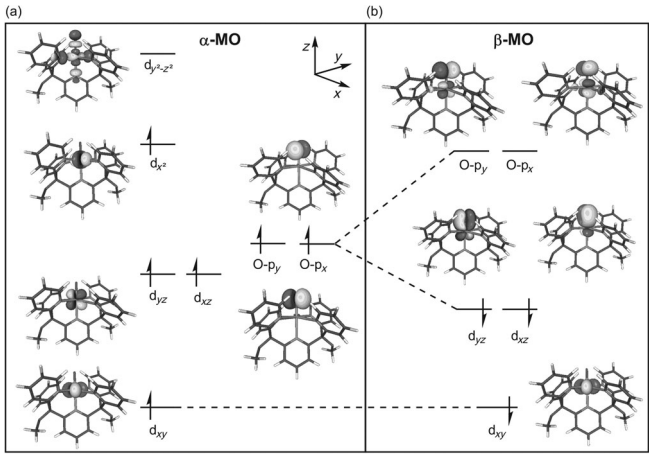

Figure 5. Natural orbitals of intermediate ^{4}**3**, the $[Co^{II}–(\cdot O\cdot)]^{2+}$ intermediate. (a) α-MOs; (b) β-MOs.

electron density distribution leads to the calculated excess of α-electron density on the terminal oxygen that we have assigned to be consistent with a Co^{II}–oxene moiety.

Whereas our interpretation of the electronic structure is plausible and places the emphasis on deriving an intuitive explanation for the observed chemical reactivity, there are alternative ways of interpreting the electronic structure. As is always the case when computed molecular orbitals are correlated to formal concepts like oxidation states, an equally valid view may be to insist on a Co^{IV}–oxo assignment invoking an unusually strong π-donation from the Lewis-basic oxo moiety into a strongly Lewis-acidic Co^{IV} center in the β-orbital space, which leads to the spin polarization at the oxygen atom. Both descriptions are legitimate and valid; we prefer the former description, as it highlights the basis of the water oxidation reactivity in a more intuitive way. More importantly, both interpretations of the electronic structure highlight the advantage of utilizing a first-row transition-metal to prepare a redox catalytic site: Whereas the doublet, low-spin spin state ^{2}**3** is the lowest energy configuration, the Co center can access the intermediate-spin configuration in ^{4}**3** with essentially no energetic penalty, as discussed above. In light of the electronic structure of the quartet state described above, this finding is easy to understand, as the high oxidation state is stabilized by intramolecular electron transfer from the oxygen to the cobalt atoms. This mechanism in turn allows for maximizing the in situ radicaloid character at the oxygen atom by engaging both Co-dπ orbitals at the same time; in second- or third-row analogues the energetic penalty of accessing such a state is much too great (see the Supporting Information for details).

Generation and release of $^3O_2$

After forming the O–O bond, two more electrons and one additional proton must be removed to complete the catalytic cycle and produce molecular dioxygen. As the cobalt center has expended all of its oxidative power to generate the Co^{II}-hydroperoxo species, it must be "recharged", that is, electrochemically oxidized. This is a significant, but intrinsic, disadvantage of mononuclear water oxidation catalysts in comparison to multimetallic systems, in which four oxidizing equivalents can be stored across multiple metal centers. Scheme 3

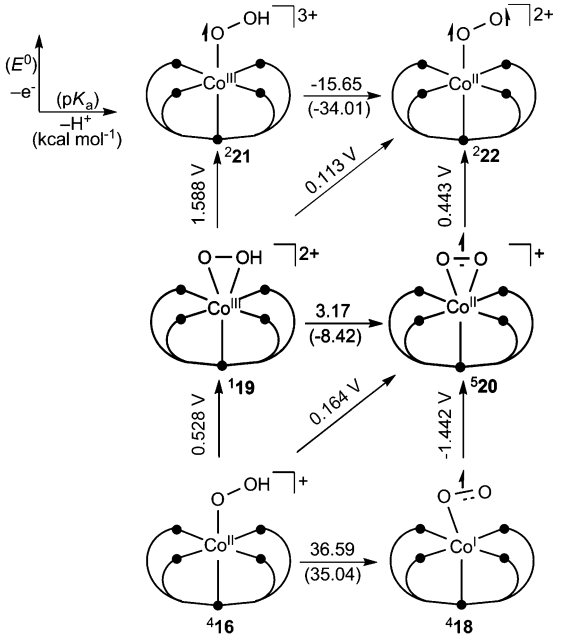

Scheme 3. Energies of the different possible intermediates in the mechanism.

summarizes the energies of the different possible intermediates. The Co^{II}–hydroperoxo complex ^{4}**16** is relatively easy to oxidize compared to the first oxidation cycle described above. Our calculations show that the removal of the first electron is directly coupled to deprotonation: Among the possible one-electron oxidized intermediates, the low-spin complex ^{1}**19** has the lowest energy with the triplet analogue ^{3}**19** being 6 kcal mol^{-1} higher in energy. The pK_a of ^{1}**19** is computed to be 3.17, however, and we consequently predict that a proton should be lost simultaneously with the oxidation at the experimental condition of pH 9.2. Interestingly, our calculations indicate that the electronic structure of the oxidized intermediate is most consistent with a Co^{II}–superoxo species, in which the Co^{II} center adopts a high-spin d^7 configuration. There is a total of 1.3 unpaired electrons distributed over the $[O_2]$ fragment to afford an overall quintet state in the intermediate ^{5}**20**. The final oxidation is again assisted by intersystem crossing at the metal to install a low-spin Co^{II} center, which is anti-ferromagnetically coupled to a loosely bound triplet dioxygen. The oxidation potential of this last step is calculated to be 0.443 V and is therefore only about 300 mV more positive than the proton-coupled first oxidation. As all these redox reactions are electrochemically irreversible and are likely not Nernstian, none of these formally computed potentials are likely to be physically meaningful. Most importantly, all oxidation events in this latter part of the catalytic cycle are predicted to occur at much more negative oxidation potential than the onset potential of ~1.3 V

discussed above and are therefore expected to progress without much difficulty at the catalytic onset potential. The catalytic cycle is completed finally with the release of triplet dioxygen and uptake of a new water substrate to return to the catalytically competent intermediate ^{4}**1**. These processes are associated with reasonable energies of −17.4 and +7.9 kcal mol^{-1}, respectively.

Conclusions

Figure 6 summarizes the mechanism that is most consistent with our calculations. The resting state ^{4}**1** is activated by a sequence of a proton-coupled single electron oxidation at a computed oxidation potential E_1° of 0.456 V followed by a second

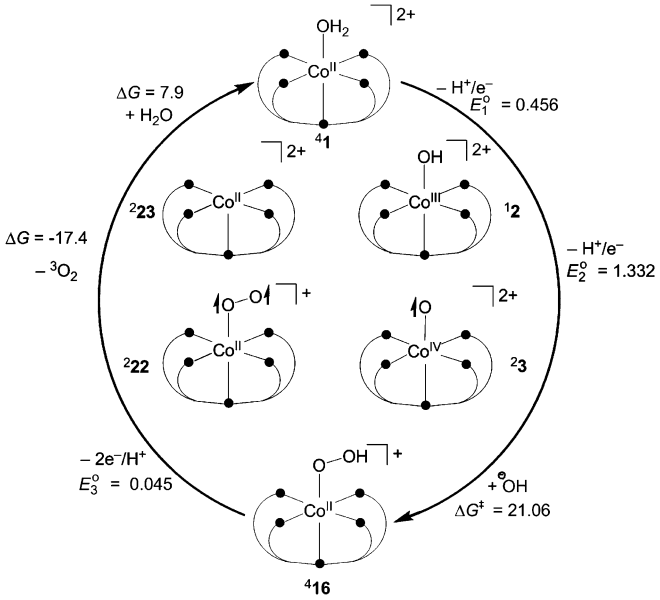

Figure 6. Proposed catalytic cycle for water oxidation.

proton-coupled oxidation at 1.332 V to afford intermediate ^{2}**3**. Whereas ^{2}**3**, is the lowest energy spin-state, the quartet state lies only 1.1 kcal mol^{-1} higher in energy, such that intermediate **3** possesses character of both spin states. The diradicaloid character within the fragment $[Co^{II}–(\cdot O\cdot)]^{2+}$ in ^{4}**3** increases the overall radical character of the oxygen fragment promoting nucleophilic attack of an anionic hydroxide substrate on the formally zero-valent oxygen atom that can be interpreted as a cobalt–oxene moiety. The spin polarization required for this unusual electronic structure is enabled by empty d-π orbitals of the highly oxidizing, formally Co^{IV}-d^5 metal center in what would be an intermediate-spin quartet configuration of the formally Co^{IV}-d^5 center. The structurally rigid Py5 ligand is responsible for generating a ligand field, in which this highly reactive state is almost isoenergetic to the low-spin doublet ground state. We examined both the intra- and intermolecular O–O bond-forming reaction pathways and found the intermolecular trajectory on the quartet potential energy surface to be most feasible with a barrier of only 21 kcal mol^{-1} to form the Co^{II}-hydroperoxo intermediate. Our calculations suggest that the remaining two oxidation steps of the overall four-electron process are much easier to accomplish than the first two and should complete spontaneously.

Acknowledgements

We thank the NSF(0116050, CHE-0645381, CHE-1001589) and the Research Corporation (Scialog Award to MHB) for support. CPB gratefully acknowledges the Alfred P. Sloan Foundation and National Sciences and Engineering Research Council of Canada for support.

Keywords: cobalt · density functional theory · photocatalysis · solar fuels · water oxidation

[1] N. S. Lewis, D. G. Nocera, *Proc. Natl. Acad. Sci. USA* **2006**, *103*, 15729.
[2] N. S. Lewis, D. G. Nocera, *Proc. Natl. Acad. Sci. USA* **2007**, *104*, 20142.
[3] J. H. Alstrum-Acevedo, M. K. Brennaman, T. J. Meyer, *Inorg. Chem.* **2005**, *44*, 6802.
[4] D. Gust, T. A. Moore, A. L. Moore, *Acc. Chem. Res.* **2001**, *34*, 40.
[5] Y. Umena, K. Kawakami, J.-R. Shen, N. Kamiya, *Nature* **2011**, *473*, 55.
[6] J. A. Gilbert, D. S. Eggleston, W. R. Murphy, D. A. Geselowitz, S. W. Gersten, D. J. Hodgson, T. J. Meyer, *J. Am. Chem. Soc.* **1985**, *107*, 3855.
[7] Y. Naruta, M. Sasayama, T. Sasaki, *Angew. Chem. Int. Ed. Engl.* **1994**, *33*, 1839; *Angew. Chem.* **1994**, *106*, 1964.
[8] M. Ledney, P. K. Dutta, *J. Am. Chem. Soc.* **1995**, *117*, 7687.
[9] J. Limburg, J. S. Vrettos, L. M. Liable-Sands, A. L. Rheingold, R. H. Crabtree, G. W. Brudvig, *Science* **1999**, *283*, 1524.
[10] T. Wada, K. Tsuge, K. Tanaka, *Angew. Chem. Int. Ed.* **2000**, *39*, 1479; *Angew. Chem.* **2000**, *112*, 1539.
[11] C. Sens, I. Romero, M. Rodriguez, A. Llobet, T. Parella, J. Benet-Buchholz, *J. Am. Chem. Soc.* **2004**, *126*, 7798.
[12] R. Zong, R. P. Thummel, *J. Am. Chem. Soc.* **2005**, *127*, 12802.
[13] Y. Xu, T. Aakermark, V. Gyollai, D. Zou, L. Eriksson, L. Duan, R. Zhang, B. Aakermark, L. Sun, *Inorg. Chem.* **2009**, *48*, 2717.
[14] Y. V. Geletii, B. Botar, P. Kogerler, D. A. Hillesheim, D. G. Musaev, C. L. Hill, *Angew. Chem. Int. Ed.* **2008**, *47*, 3896; *Angew. Chem.* **2008**, *120*, 3960.
[15] A. Sartorel, M. Carraro, G. Scorrano, R. De Zorzi, S. Geremia, N. D. McDaniel, S. Bernhard, M. Bonchio, *J. Am. Chem. Soc.* **2008**, *130*, 5006.
[16] R. Brimblecombe, A. Koo, G. C. Dismukes, G. F. Swiegers, L. Spiccia, *J. Am. Chem. Soc.* **2010**, *132*, 2892.
[17] L. Francas, X. Sala, E. Escudero-Adan, J. Benet-Buchholz, L. Escriche, A. Llobet, *Inorg. Chem.* **2011**, *50*, 2771.
[18] H.-W. Tseng, R. Zong, J. T. Muckerman, R. Thummel, *Inorg. Chem.* **2008**, *47*, 11763.
[19] J. J. Concepcion, J. W. Jurss, J. L. Templeton, T. J. Meyer, *J. Am. Chem. Soc.* **2008**, *130*, 16462.
[20] N. D. McDaniel, F. J. Coughlin, L. L. Tinker, S. Bernhard, *J. Am. Chem. Soc.* **2008**, *130*, 210.
[21] J. D. Blakemore, N. D. Schley, D. Balcells, J. F. Hull, G. W. Olack, C. D. Incarvito, O. Eisenstein, G. W. Brudvig, R. H. Crabtree, *J. Am. Chem. Soc.* **2010**, *132*, 16017.
[22] A. Savini, G. Bellachioma, G. Ciancaleoni, C. Zuccaccia, D. Zuccaccia, A. Macchioni, *Chem. Commun.* **2010**, *46*, 9218.
[23] W. C. Ellis, N. D. McDaniel, S. Bernhard, T. J. Collins, *J. Am. Chem. Soc.* **2010**, *132*, 10990.
[24] J. L. Fillol, Z. Codolà, I. Garcia-Bosch, L. Gómez, J. J. Pla, M. Costas, *Nat. Chem.* **2011**, *3*, 807.
[25] M. K. Coggins, M.-T. Zhang, A. K. Vannucci, C. J. Dares, T. J. Meyer, *J. Am. Chem. Soc.* **2014**, *136*, 5531.
[26] D. Wang, J. T. Groves, *Proc. Natl. Acad. Sci. USA* **2013**, *110*, 15579.
[27] D. K. Dogutan, R. McGuire, D. G. Nocera, *J. Am. Chem. Soc.* **2011**, *133*, 9178.
[28] M. Z. Ertem, C. J. Cramer, *Dalton Trans.* **2012**, *41*, 12213.

[29] F. Acuña-Parés, M. Costas, J. M. Luis, J. Lloret-Fillol, *Inorg. Chem.* **2014**, *53*, 5474.
[30] F. Acuña-Parés, Z. Codolà, M. Costas, J. M. Luis, J. Lloret-Fillol, *Chem. Eur. J.* **2014**, *20*, 5696.
[31] D. J. Wasylenko, C. Ganesamoorthy, J. Borau-Garcia, C. P. Berlinguette, *Chem. Commun.* **2011**, *47*, 4249.
[32] D. J. Wasylenko, R. D. Palmer, E. Schott, C. P. Berlinguette, *Chem. Commun.* **2012**, *48*, 2107.
[33] T. A. Betley, Q. Wu, T. Van Voorhis, D. G. Nocera, *Inorg. Chem.* **2008**, *47*, 1849.
[34] P. E. M. Siegbahn, R. H. Crabtree, *J. Am. Chem. Soc.* **1999**, *121*, 117.
[35] M. Lundberg, M. R. A. Blomberg, P. E. M. Siegbahn, *Inorg. Chem.* **2004**, *43*, 264.
[36] X. Yang, M.-H. Baik, *J. Am. Chem. Soc.* **2004**, *126*, 13222.
[37] X. Yang, M.-H. Baik, *J. Am. Chem. Soc.* **2006**, *128*, 7476.
[38] S. Ghosh, M.-H. Baik, *Angew. Chem. Int. Ed.* **2012**, *51*, 1221; *Angew. Chem.* **2012**, *124*, 1247.
[39] S. Ghosh, M. H. Baik, *Inorg. Chem.* **2011**, *50*, 5946.
[40] Z. Chen, J. J. Concepcion, X. Hu, W. Yang, P. G. Hoertz, T. J. Meyer, *Proc. Natl. Acad. Sci. USA* **2010**, *107*, 7225 – 7229.
[41] J. J. Concepcion, J. W. Jurss, M. K. Brennaman, P. G. Hoertz, A. O. T. Patrocinio, N. Y. Murakami Iha, J. L. Templeton, T. J. Meyer, *Acc. Chem. Res.* **2009**, *42*, 1954.
[42] J. W. Jurss, J. J. Concepcion, J. M. Butler, K. M. Omberg, L. M. Baraldo, D. G. Thompson, E. L. Lebeau, B. Hornstein, J. R. Schoonover, H. Jude, J. D. Thompson, D. M. Dattelbaum, R. C. Rocha, J. L. Templeton, T. J. Meyer, *Inorg. Chem.* **2012**, *51*, 1345.
[43] D. Moonshiram, I. Alperovich, J. J. Concepcion, T. J. Meyer, Y. Pushkar, *Proc. Natl. Acad. Sci. USA* **2013**, *110*, 3765.
[44] R. G. Parr, W. Yang, *Density Functional Theory of Atoms and Molecules*; Oxford University Press, New York, **1989**.
[45] T. Ziegler, *Chem. Rev.* **1991**, *91*, 651.
[46] 7.7, J.; Schrödinger, Inc., New York, NY, **2013**.
[47] A. D. Becke, *Phys. Rev. A* **1988**, *38*, 3098.
[48] A. D. Becke, *J. Chem. Phys.* **1993**, *98*, 5648.
[49] C. Lee, W. Yang, R. G. Parr, *Phys. Rev. B* **1988**, *37*, 785.
[50] J. C. Slater, *Quantum Theory of Molecules and Solids, Vol. 4: The Self-Consistent Field for Molecules and Solids*, McGraw-Hill, New York, **1974**.
[51] S. H. Vosko, L. Wilk, M. Nusair, *Can. J. Phys.* **1980**, *58*, 1200.
[52] P. J. Hay, W. R. Wadt, *J. Chem. Phys.* **1985**, *82*, 270.
[53] P. J. Hay, W. R. Wadt, *J. Chem. Phys.* **1985**, *82*, 299.
[54] T. H. Dunning, Jr., *J. Chem. Phys.* **1989**, *90*, 1007.
[55] C. M. Cortis, R. A. Friesner, *J. Comput. Chem.* **1997**, *18*, 1570.
[56] C. M. Cortis, R. A. Friesner, *J. Comput. Chem.* **1997**, *18*, 1591.
[57] S. R. Edinger, C. Cortis, P. S. Shenkin, R. A. Friesner, *J. Phys. Chem. B* **1997**, *101*, 1190.
[58] A. A. Rashin, B. Honig, *J. Phys. Chem.* **1985**, *89*, 5588.
[59] M. D. Tissandier, K. A. Cowen, W. Y. Feng, E. Gundlach, M. H. Cohen, A. D. Earhart, J. V. Coe, T. R. Tuttle, Jr., *J. Phys. Chem. A* **1998**, *102*, 7787.
[60] C. P. Kelly, C. J. Cramer, D. G. Truhlar, *J. Phys. Chem. B* **2006**, *110*, 16066.
[61] M. Zhang, M. de Respinis, H. Frei, *Nat. Chem.* **2014**, *6*, 362.
[62] Q. Yin, J. M. Tan, C. Besson, Y. V. Geletii, D. G. Musaev, A. E. Kuznetsov, Z. Luo, K. I. Hardcastle, C. L. Hill, *Science* **2010**, *328*, 342.
[63] F. Jiao, H. Frei, *Angew. Chem. Int. Ed.* **2009**, *48*, 1841; *Angew. Chem.* **2009**, *121*, 1873.
[64] M. W. Kanan, D. G. Nocera, *Science* **2008**, *321*, 1072.
[65] F. F. Pfaff, S. Kundu, M. Risch, S. Pandian, F. Heims, I. Pryjomska-Ray, P. Haack, R. Metzinger, E. Bill, H. Dau, P. Comba, K. Ray, *Angew. Chem. Int. Ed.* **2011**, *50*, 1711; *Angew. Chem.* **2011**, *123*, 1749.
[66] M.-H. Baik, R. A. Friesner, *J. Phys. Chem. A* **2002**, *106*, 7407.
[67] D. J. Wasylenko, H. M. Tatlock, L. S. Bhandari, J. R. Gardinier, C. P. Berlinguette, *Chem. Sci.* **2013**, *4*, 734.
[68] P. Hendry, A. Ludi, *Adv. Inorg. Chem.* **1990**, *35*, 117.
[69] H. U. D. Wiesendanger, W. H. Jones, C. S. Garner, *J. Chem. Phys.* **1957**, *27*, 668.
[70] J. Lilie, N. Shinohara, M. G. Simic, *J. Am. Chem. Soc.* **1976**, *98*, 6516.
[71] J. Xie, Q.-X. Zhou, C. Li, W. Wang, Y.-J. Hou, B.-W. Zhang, X. Wang, *Chem. Commun.* **2014**, *50*, 6520 – 6522.
[72] K. Tanaka, H. Isobe, S. Yamanaka, K. Yamaguchi, *Proc. Natl. Acad. Sci. USA* **2012**, *109*, 15600.
[73] T. Wada, H. Ohtsu, K. Tanaka, *Chem. Eur. J.* **2012**, *18*, 2374.
[74] V. K. Yachandra, K. Sauer, M. P. Klein, *Chem. Rev.* **1996**, *96*, 2927.
[75] P. E. M. Siegbahn, *Chem. Eur. J.* **2006**, *12*, 9217.
[76] J. Messinger, *Phys. Chem. Chem. Phys.* **2004**, *6*, 4764.
[77] K. Kobayashi, H. Ohtsu, T. Wada, T. Kato, K. Tanaka, *J. Am. Chem. Soc.* **2003**, *125*, 6729.
[78] A. Kimoto, K. Yamauchi, M. Yoshida, S. Masaoka, K. Sakai, *Chem. Commun.* **2012**, *48*, 239.
[79] T. S. Dowers, D. A. Rock, D. A. Rock, J. P. Jones, *J. Am. Chem. Soc.* **2004**, *126*, 8868.
[80] K. Auclair, Z. Hu, D. M. Little, P. R. Ortiz de Montellano, J. T. Groves, *J. Am. Chem. Soc.* **2002**, *124*, 6020.
[81] J. T. Groves, G. A. McClusky, R. E. White, M. J. Coon, *Biochem. Biophys. Res. Commun.* **1978**, *81*, 154.
[82] F. P. Guengerich, T. L. MacDonald, *FASEB J.* **1990**, *4*, 2453.
[83] J. P. Foster, F. Weinhold, *J. Am. Chem. Soc.* **1980**, *102*, 7211.
[84] A. E. Reed, F. Weinhold, *J. Chem. Phys.* **1985**, *83*, 1736.

Received: September 19, 2014
Published online on January 14, 2015